



Article

Energy Assessment of Alternative City Bus Lines: A Case Study in Gijón, Spain

Jose Diaz * , Borja Pérez and Francisco J. Fernández 

Polytechnic School of Engineering, University of Oviedo, 33204 Gijón, Spain; uo257285@uniovi.es (B.P.); javierfernandez@uniovi.es (F.J.F.)

* Correspondence: diazjose@uniovi.es

Abstract: The progressive substitution of traditional buses with electric ones in urban public transport constitutes a fundamental challenge towards sustainable mobility. This paper presents a methodological approach to assess energy consumption in urban bus networks, focusing on a city with varied topography and examining alternative bus lines for similar trips. Utilizing a quasi-static longitudinal model, real GPS data, and open access terrain models, the analysis aims to provide a nuanced understanding of energy performance, considering factors such as stop characteristics, gradients, and driving styles. The influence of driving style on commercial speed is observed to be modest, yet significant, in terms of energy efficiency. This research identifies the most advantageous line for transitioning from Internal Combustion Engine (ICE) to Electric Motor (EM) powertrains, resulting in a significant 68% reduction in energy consumption. Beyond specific line details, this methodology offers insights applicable to medium-sized cities, emphasizing efficient route prioritization and providing enhanced user information for informed decisions in the context of sustainable transportation solutions.

Keywords: sustainable mobility; urban public transport; bus line comparison; energy efficiency



Citation: Diaz, J.; Pérez, B.; Fernández, F.J. Energy Assessment of Alternative City Bus Lines: A Case Study in Gijón, Spain. *Sustainability* **2024**, *16*, 4101. <https://doi.org/10.3390/su16104101>

Academic Editor: Marilisa Botte

Received: 9 April 2024

Revised: 8 May 2024

Accepted: 12 May 2024

Published: 14 May 2024



Copyright: © 2024 by the authors. Licensee MDPI, Basel, Switzerland. This article is an open access article distributed under the terms and conditions of the Creative Commons Attribution (CC BY) license (<https://creativecommons.org/licenses/by/4.0/>).

1. Introduction

The gradual replacement of traditional buses with electric buses in urban public transport represents a fundamental challenge towards sustainable mobility. This transition is not only environmentally responsible but also economically strategic in the long term. It is necessary to adopt a progressive approach, so that cities can systematically integrate electric buses into their existing fleets, reducing initial investment risks. Additionally, this gradual implementation allows for the development of necessary infrastructure, such as charging stations, and gives stakeholders time to adapt to an evolving technology. As the electric bus network expands, operating costs are expected to decrease, making the economic arguments for sustainable public transport increasingly compelling.

Therefore, for any city, a meticulous analysis of the various bus routes and their corresponding driving cycles is essential. This comprehensive assessment has a dual purpose: to evaluate the energy performance of buses under various conditions and to identify specific routes that are most conducive to the transition. By understanding the unique demands of each route, transport authorities can strategically prioritize the deployment of electric buses on lines where they can maximize efficiency and economic viability, ensuring a seamless and sustainable integration into the broader urban transport system. Additionally, this microscale analysis allows users to make informed decisions between the various public transportation options available, fostering a community-wide commitment to sustainability while individuals contribute to the success of green transportation solutions.

A local route analysis, which considers orographic particularities and incorporates driving cycles, serves as a crucial method for estimating vehicle emissions and energy consumption. Driving cycles are widely adopted as a reference for evaluating energy consumption and emissions in road transport vehicles. This approach is particularly relevant

for evaluating and optimizing electric vehicle technologies, given the substantial differences in torque, power characteristics, transmission efficiency, and regenerative braking compared to conventional transmissions.

In Spain, public transport is used by 22% of the population, and, in the city of Gijón, with 274,000 habitants, the public urban transport company is responsible for the transport of almost 20 million passengers per year [1,2]. However, as in a large majority of cities, the use of electric buses is still in a testing stage. Although, compared to other cities in the region, Gijón does not have a pronounced relief, there is an appreciable difference in altitude between the center of the city, close to the coastal façade, and the southern periphery with an altitude exceeding 60 m above the sea level.

An examination of the literature reveals a demand for knowledge about the operational characteristics of urban bus networks to guide their transition to more sustainable transportation modes. However, information on representative driving cycles for specific cities or lines is scarce. While the study of driving cycles for urban bus routes were uncommon until recent years, there is now a clear growing trend for various types of buses. Most existing studies traditionally focused on conventional propulsion systems, although some relate to electric or hybrid buses, such as the case study of suburban buses in Finland [3]. Research into new forms of mobility and energy technologies has highlighted the need to consider local driving cycles, as seen in the case of energy accumulation using supercapacitors for buses in Hong Kong [4] or electric scooters in Oxford [5].

The availability of GPS data and Open Data policies provide an opportunity to enhance our knowledge of the operation of urban bus lines. These technologies currently facilitate the collection of vehicle speed data on roads. The increasing availability of real data and the development of IoT and Big Data enable open access to this information [6–8]. Most driving cycles used in these studies are either standardized, like the SORT cycles [9]; synthetic, where a standard cycle is adapted to specific bus line parameters [10]; semi-synthetic, where real trip recordings are modified for considering changing driving conditions [11]; or real cycles [12]. Each approach has its advantages and disadvantages, and the choice depends on factors such as the scale of the intended analysis, and the availability of detailed data, as well as the goals of the research. In particular, the use of real data has been identified as the most suitable for a city bus analysis [13]. However, none of these studies has addressed the comparison of equivalent bus routes and are limited to single bus lines in cities like Jerusalem, Bogotá, and Liaocheng [10–12].

The road gradient significantly impacts bus operational performance, but its consideration in urban bus lines is still infrequent. While acceptable in flat cities, it becomes crucial in areas with a more pronounced relief. Studies tend to overlook the impact of road gradients, despite their effects on vehicle performance. Information about the road elevation is crucial for evaluating the driving performance of vehicles, particularly buses and other heavy vehicles [14]. Some studies oriented towards vehicle design, energy consumption minimization, and the optimization of the powertrain for heavy vehicles highlight the importance of considering road gradients in the development of a synthetic driving cycle [15]. Notably, road gradient and vehicle mass information was conveniently included in a driving cycle for garbage trucks [16]. Research on urban bus driving patterns often overlooks the influence of road gradients, despite their impact on vehicle behavior and driver actions [17,18]. This makes it essential for a local-scale analysis. Consequently, this study deliberately chooses bus routes offering similar services but traversing different terrains and traffic conditions. The aim is to propose a more realistic assessment of improvement strategies by considering the unique features of the city.

In recent years, there has been a growing interest in the comparative analysis of urban transport lines within the same city; however, the provided overview remains incomplete. Some studies compare different network designs, aiming to assess service efficiency in aspects such as commercial speed and headway, but overlooking energy costs and the impact of terrain, among other driving cycle characteristics [19]. Similar limitations are evident in studies focusing on specific cities like Utrecht or Istanbul [20,21]. An insightful

study conducted in Singapore employed synthetic cycles to evaluate the specific energy consumption of a hypothetical fleet of electric vehicles [22]. Three bus sizes and 350 lines were considered, revealing significant differences between lines. For a 12.5-ton single-deck non-articulated bus, the overall specific consumption was 160 kWh/100 km, but, depending on the route, it could vary between 110 and 220 kWh/100 km. However, a comparison between lines providing equivalent services is not conducted, preventing an assessment of energy efficiency concerning the actual service delivered.

This paper seeks to fill a gap in real-world operational data for bus driving in small- or medium-sized cities with steep terrain. A novel analysis is conducted, comparing bus lines with varying energy consumption while providing a similar service. The major contributions of this paper are summarized as follows:

1. This work proposes a microscale analysis of bus routes, based on a detailed examination of driving cycles and orographic particularities, to evaluate energy performance and identify opportunities to sustainable transportation.
2. The novel methodology integrates low-cost GPS acquisition and free Open Data to enhance our understanding of urban bus network operations. By leveraging real and detailed data, this study fills the knowledge gap regarding representative driving cycles for specific cities or bus lines.
3. This work addresses the oversight of the road gradient in previous research on urban bus driving. By deliberately choosing bus routes with varying terrains and traffic conditions, this study offers a more realistic assessment of improvement strategies.

The rest of the article is organized as follows: Section 2 describes the selection of bus lines, the construction of models for the vehicles, and the generation of driving cycles. Section 3 presents the results obtained for the different bus lines and powertrains, comparing them. Subsequently, Section 4 analyzes how the different characteristics of driving cycles affect fuel consumption through the dissipative resistances experienced by the vehicle. Additionally, it demonstrates how the generated knowledge can be applied in a rational deployment of new transportation systems and for user guidance. Finally, conclusions are drawn in Section 5.

2. Materials and Methods

2.1. Bus Lines Selection

The primary urban bus routes in the city follow both a west–east and south–east trajectory, typically passing through the city center. This arrangement caters to the densely populated neighborhoods in the southern and western parts of the city, linking them with the northern coastal center and the eastern service area housing major sports facilities, universities, and hospitals. In Figure 1, notable variations in elevation are depicted within city’s topography, showing a difference exceeding 60 m between the city center and the southern periphery. In contrast, the western periphery has a lower elevation, akin to the central and eastern regions. Consequently, an insightful analysis should focus on the L02, L10, and L15 lines, which provide similar services along the south–north–east axis but exhibit distinct features.

Both L02 and L10 operate between the south suburban hub and the city central hospital. However, the former avoids the city center, resulting in a more level altimetric profile. The L15 connects the southern suburban outskirts to the hospital, mirroring the L10 route but traversing slightly higher areas. These three bus lines offer a good basis for study and comparison due to variations in length, elevation, and usage, despite providing a similar service. Notably, they rank among the most utilized in the city’s public bus service, as detailed in Table 1. This study considers the round trip for each line, constituting a closed cycle with identical starting and ending points.

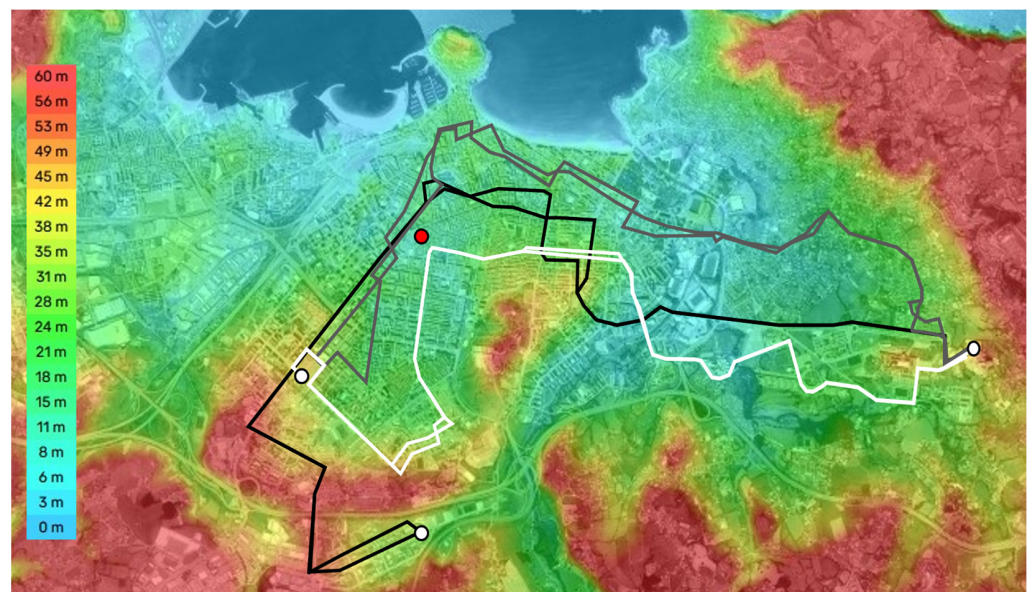


Figure 1. Aerial photograph of Gijón indicating the relief contours and bus lines: L02 (white), L10 (grey), and L15 (black). Terminus stops (white dots) and a sample user location (red dot) are shown.

Table 1. Characteristics of the bus lines considered in this study [1].

Bus Line	Length (km)	Elevation: Min–Max (m)	Cumulative Elev. Gain (m)	Boarding Stations	Usage (10 ³ pass./year)	Usage Ranking
L02	18.5	8–50	200	58	515	10th
L10	18.4	3–50	103	60	1970	4th
L15	22.5	3–62	252	64	2180	3th

2.2. Bus Vehicle Modelling

A one-dimensional equation for the longitudinal dynamics of a vehicle with a constant mass m and varying speed $v(t)$ is adopted:

$$F_t = m \frac{dv}{dt} + F_a + F_r + F_g, \quad (1)$$

where F_a is the aerodynamic resistance, F_r the rolling resistance, and F_g the gravity force. The traction force of the vehicle F_t is the force provided by the motor minus the friction losses and the inertia of the moving parts inside the powertrain. As seen in Equation (1), traction force compensates the resistances and provides the required acceleration to the vehicle.

The aerodynamic resistance for a prismatic body with a frontal area A_f and a constant drag coefficient c_d is considered:

$$F_a = \frac{1}{2} c_d A_f \rho_a v^2, \quad (2)$$

where ρ_a is the air density. The rolling resistance is modeled as:

$$F_r = c_r m g \cos(\alpha), \quad (3)$$

where c_r represents the friction coefficient, which depends on some variables such as vehicle speed, tire pressure, or road conditions, but their variability is small and c_r is assumed to be constant. The gravitational force is given by:

$$F_g = m g \sin(\alpha). \quad (4)$$

Provided that the speed of the vehicle $v(t)$ and the gradient of the road $\alpha(t)$ are known, the traction force delivered by the powertrain $F_t(t)$ can be calculated from Equations (1)–(4). Then, motor torque $T_m(t)$ and rotation speed $\omega(t)$ can be obtained from:

$$T_m = \frac{r_w}{i_{gb}(k) \eta} F_t, \quad (5)$$

and

$$\omega_m = \frac{i_{gb}(k)}{r_w} v, \quad (6)$$

where r_w is the wheel radius, $i_{gb}(k)$ the gearbox ratio for gear number k , and η the gearbox efficiency. The inertia of the rotating masses is considered by increasing the mass of the vehicle. The energy consumption of the motor is obtained from the fuel consumption characteristic map in the case of a powertrain with internal combustion engine and from the efficiency map in the case of a powertrain with electric motor. In both cases, the energy consumption is determined from the rotation speed and the torque:

$$\dot{E}_m = f(T_m, \omega_m). \quad (7)$$

For electric powertrains, the battery charge–discharge system efficiency is also considered.

The proposed model was implemented using MatLab/Simulink R2020b. The Quasi-Static Simulation (QSS) toolbox enables the backward quasi-static modeling and simulation of both conventional and alternative powertrains [23]. It incorporates blocks featuring static efficiency maps for powertrain components and control logics. While originally designed for rapid sizing, optimization, and verification of powertrains, it can be effectively customized for testing against real-world driving cycles. In adapting the existing models within the QSS library, modifications were made to include route gradient. The simulations utilized a timestep of 1 s across all scenarios.

The complete model is depicted in Figure 2 where the block scheme used for comparison between conventional and electric powertrains is shown. On one hand, the internal combustion engine (ICE) version is composed of four blocks: vehicle, gearbox, engine, and fuel tank. On the other hand, the electric motor (EM) model is composed of four blocks: vehicle, gearbox, motor, and battery. On the left side of the picture, the driving cycle block feeds both powertrains with velocity and gradient profiles.

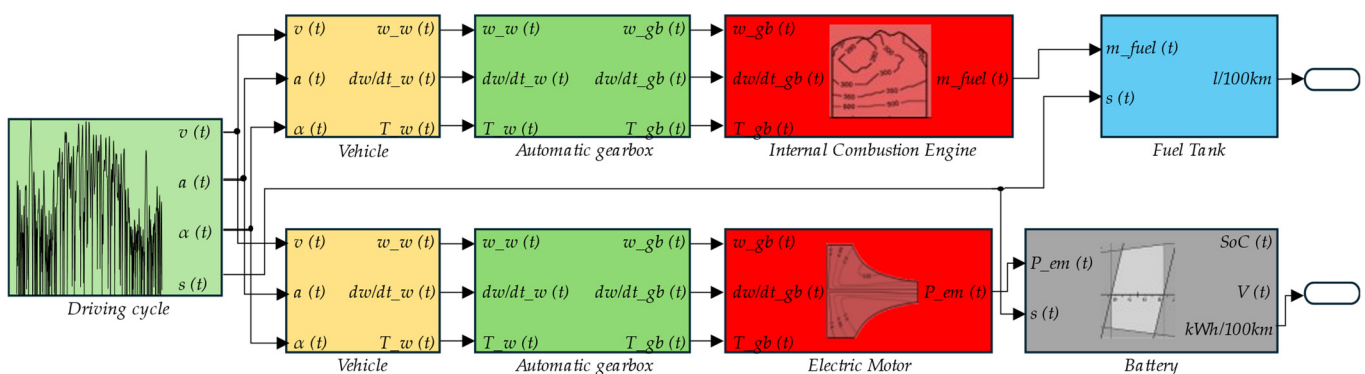


Figure 2. Block diagram showing sub-systems for internal combustion engine powertrain (top) and electric motor powertrain (bottom) models.

The internal combustion engine (ICE) and the electric motor (EM) models are based on Mercedes-Benz Citaro and eCitaro characteristics [24]. The required technical data are summarized in Table 2. Data from ZF Friedrichshafen were used for ICE and EM transmissions [25]. For the internal combustion model, a 220 kW engine from Mercedes (OM 936) was chosen since it is often found in Citaro units [24]. In the case of the electric model, a 250 kW AxTrax AVE 130 motor was adopted [25]. Both propulsion systems were modeled using the basic QSS models, taking into account their actual torque curves and power characteristics. The effective masses of the vehicles were determined by considering the maximum weights and passenger capacity. Despite logical differences in weight, propulsion, and transmission, both vehicles share comparable dimensions and performance attributes, enhancing the significance of the comparison.

Table 2. Parameters adopted for the simulation of internal combustion and electric vehicles.

Vehicle Parameter	ICE	EM
Maximum mass (kg)	18,000	20,000
Maximum passenger capacity (-)	89	78
Ridership (-)	34	34
Passenger mass (kg)	91	91
Effective mass (kg)	13,000	16,000
Frontal area, A_f (m ²)	5.9	5.9
Aerodynamic drag coefficient c_d (-)	0.8	0.8
Rolling friction coefficient c_r (-)	0.009	0.009
Wheel diameter (m)	0.956	0.956
Number of gearbox ratios (-)	6	1
Gearbox ratios, $i_{GB}(k)$ (-)	[3.36 1.91 1.42 1.00 0.72 0.62]	22.66
Upshifting velocities (km/h)	[19 33 44 62 86]	-
Downshifting velocities (km/h)	[6 19 24 29 59]	-

2.3. Driving Cycle Modelling

Various driving cycles, both legislative and non-legislative, have been developed globally. These include standards from cities like New York, Paris, and Braunschweig, often chosen based on similarity to the study case. Normalized SORT cycles were designed to replicate typical urban bus driving conditions, ensuring consistent evaluations across routes and cities. SORT 1 reflects moderate city driving (commercial speed 12.6 km/h), SORT 2 depicts aggressive driving on congested routes (commercial speed 18.6 km/h), and SORT 3 combines urban and suburban driving (commercial speed 26.3 km/h). However, these cycles may not fully represent real-world scenarios, leading operators and manufacturers to develop improved tests like MLTB (based on London's route 159). Yet, the most accurate approach remains considering actual driving cycles of the specific location.

The acquisition of speed data for the selected bus lines was carried out using an on-board GPS datalogger at 1 Hz sampling frequency on a hybrid Mercedes-Benz Citaro. Raw velocity data were processed, preserving maximum velocities and total journey duration in order to estimate a 3% of missing values. The measurements were carried out in different days for each line in order to select a representative cycle for the study. At least two trips were conducted for each line and each driving condition to verify the representativeness of the cycle. Figure 3 illustrates a comparison of the speed profile for line L10 in three different scenarios: late afternoon on a weekday, late morning on a weekday, and late afternoon on a holiday. Table 3 summarizes the main differences between the considered scenarios. It is observed that the late morning and late afternoon hours on weekdays are very similar and much more critical than on holidays. Similar results were obtained for lines L02 and L15. Since most services are concentrated on weekdays, the weekday afternoon cycles for each line were selected as representative in this study.

The road gradient for each cycle was calculated from Google Earth Pro's elevation graphs and digitalized. The primary source of these data is the Shuttle Radar Topography

Mission (SRTM). Some minor corrections to the raw data had to be made in the case of lane overlap in elevated crossings and tunnels. Finally, road gradient was related to the time through the position. The resulting driving cycles (t , $v(t)$, $a(t)$) were fed to the model.

In order to enrich the evaluation of the real bus lines, the SORT 1 was used. It involves a series of predefined driving conditions, including acceleration (1.03 , 0.77 , and 0.62 m/s²), cruising (20 , 30 , and 40 km/h), deceleration (0.8 m/s²), and stop (20 s) phases, representing typical urban driving patterns. The SORT driving cycles provide a consistent benchmark for assessing and comparing the environmental impact of different vehicles under on-road conditions [17,18]. The basic sequence is repeated until a distance of 22 km is covered, making it comparable to the longer real line, L15.

Table 3. Main parameters of the driving cycles for line L10.

Parameter	Weekday Afternoon	Weekday Morning	Holiday Afternoon
Boarding stops per km	2.8	2.6	1.7
Total stops per km	7.5	6.9	4.7
Travel time (min)	87	83	64
Average speed (km/h)	15.5	16.5	19.7
Commercial speed (km/h)	12.7	13.2	17.2

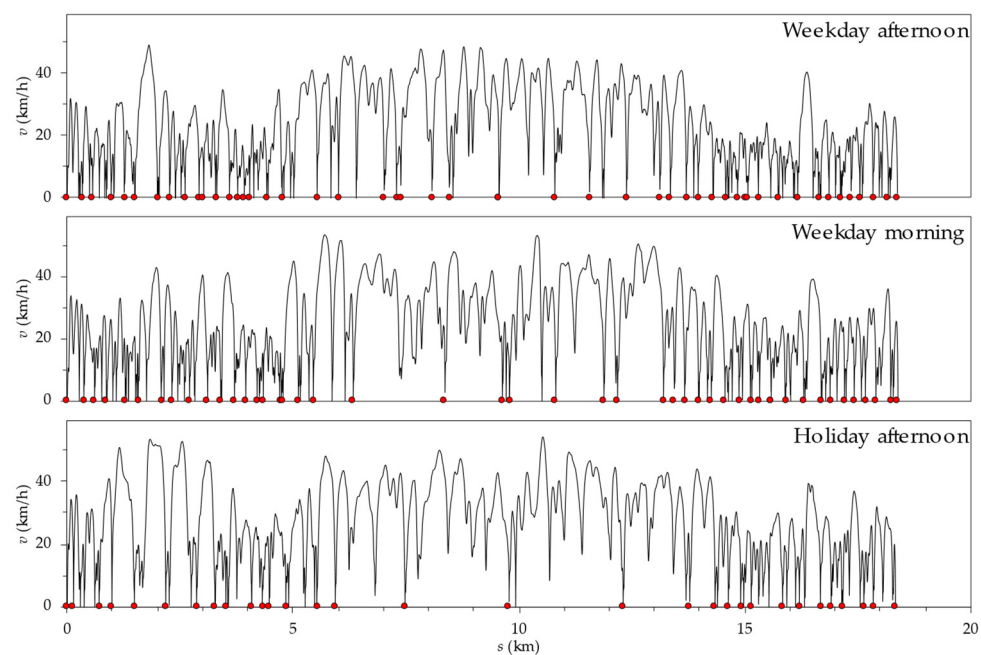


Figure 3. Velocity profile comparison for line L10. Passenger stops marked with red dots.

Additionally, with the aim of analyzing the effect of driving style, semi-synthetic cycles were constructed as counterparts to the previous cycles, imposing a maximum speed limitation of 30 km/h. This limit was chosen considering the traffic regulations trend in Spain to reduce the maximum speed on streets with a single lane in each direction within urban areas [26]. The distance traveled within a specified time was recalculated, taking into account the imposed speed limit.

3. Results

The acquisition of velocity profiles during real driving cycles was conducted twice for each route, always during the central hours of the afternoon on a weekday. The velocity and elevation profiles, for both real and SORT cycles, are represented as a function of the distance traveled in Figure 4. Passenger loading and unloading stops are indicated by red dots, while the remaining zero velocity points are due to traffic lights or traffic delays

primarily caused by queues to access roundabouts. Additionally, Table 4 summarizes the main parameters that can be derived from the profiles.

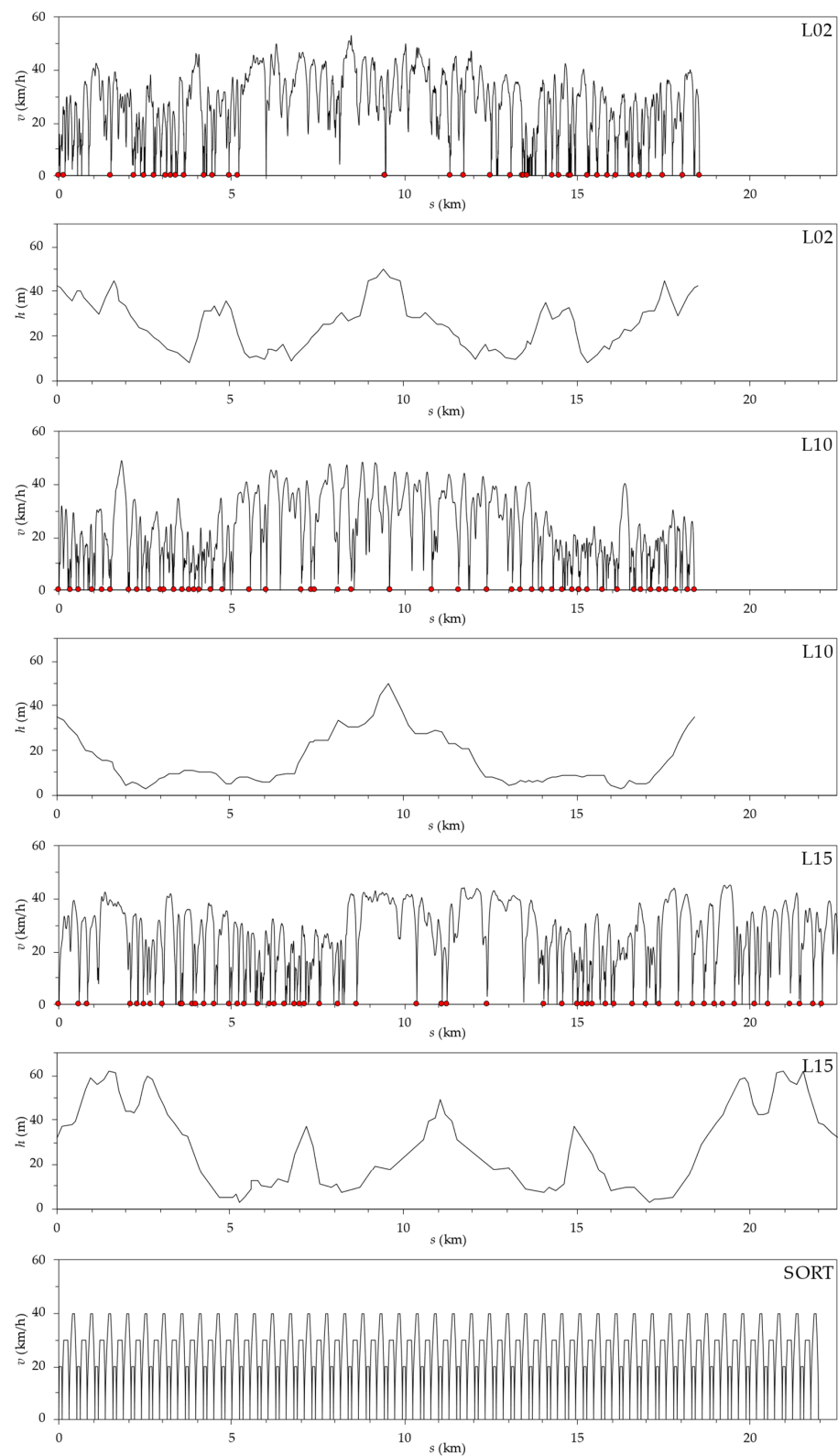


Figure 4. Velocity and elevation profiles for the main driving cycles considered in this study Passenger stops marked with red dots.

Table 4. Main parameters of the driving cycles ¹.

Parameter	L02	L10	L15	SORT 1
Boarding stops per km	2.0	2.8	2.5	-
Total stops per km	5.6	7.5	6.4	5.8
Travel distance (km)	18.5	18.4	22.5	22.0
Travel time (min)	75 (80)	87 (92)	92 (102)	105 (108)
Commercial speed (km/h)	14.9 (13.9)	12.7 (12.0)	14.7 (13.2)	12.6 (12.2)
v_{avg} (km/h)	20.4 (16.9)	15.5 (14.5)	18.5 (16.9)	20.7 (19.7)
$v_{10\%}$ (km/h)	0.0 (0.0)	0.0 (0.0)	0.0 (0.0)	0.0 (0.0)
$v_{25\%}$ (km/h)	0.0 (1.8)	2.1 (2.1)	1.7 (1.7)	0.0 (0.0)
$v_{50\%}$ (km/h)	10.6 (10.6)	9.6 (9.6)	11.2 (11.2)	8.0 (8.0)
$v_{75\%}$ (km/h)	26.4 (26.3)	19.6 (19.6)	25.7 (25.7)	21.2 (21.2)
$v_{90\%}$ (km/h)	36.0 (30.0)	32.5 (30.0)	36.0 (30.0)	30.0 (30.0)
a^+_{avg} (m/s ²)	0.34 (0.35)	0.31 (0.31)	0.31 (0.33)	0.76 (0.79)
a^-_{avg} (m/s ²)	0.44 (0.46)	0.37 (0.37)	0.40 (0.47)	0.80 (0.80)
α^+_{avg} (%)	2.5	1.3	2.8	0.0
α^-_{avg} (%)	2.5	1.1	2.5	0.0
Braking distance (%)	40 (38)	37 (33)	37 (37)	23 (18)

¹ Average and percentile values are relative to elapsed time; values in brackets correspond to the modified driving cycles with $v_{max} = 30$ km/h.

The real velocity profile does not exceed 50 km/h in any case. It is also observed that the central sections of all lines have a lower number of stops. These sections correspond to the portion of the route carried out in the eastern periphery, near the hospital. Additionally, line L15 has a zone with fewer stops at the beginning and the end of the route, corresponding to the connection between the southern periphery and the city. In peripheral areas, the number of traffic lights and roundabouts is lower, and the probability of stopping at a passenger stop is also reduced. Therefore, despite the three lines having a similar number of potential boarding stops (approximately 60 each), the effective number of stops per distance traveled is much lower in L02, in line with the SORT 1 value. This is because almost half of the route corresponds to the eastern periphery. The number of stops per distance traveled for L15 is lower than for L10 due to the trajectory through the southern periphery at the beginning and end of each journey.

Elevation profiles also reveal significant differences between lines due to their routes. In general, the overall profile for the L10 outbound journey consists of a descent and ascent, while line L02 passes through an intermediate elevation peak as it skirts the city to the south, crossing the mountainous ridge that separates the south and east areas of the city. Line L15 is similar to L10 but exhibits an additional high elevation peak, as it starts outside the city and must overcome the hill bordering the city to the south. In all cases, elevation profiles for the outbound and return journeys are essentially symmetrical, as both routes

are very similar, although not identical due mainly to variations derived from one-way streets. Consistent with the previous analysis, the average gradients are higher on line L15, followed by L02 and L10. Elevation is not considered for the SORT cycle since it is a theoretical cycle that does not account for road gradients.

The energy consumption calculated using the proposed model for the different driving cycles and the two considered powertrains are presented in Table 5. Total CO₂ emissions are also estimated using the 0.31 and 0.27 kgCO₂/kWh factors for fuel and electricity, respectively [27,28]. As can be seen, the consumption of the three real lines is lower than that of the SORT 1 for both powertrains. Line L10 shows a significantly lower consumption than SORT 1, roughly 10% lower for ICE and 15% lower for EM. The results presented in Table 5 align with values previously reported in the literature. For instance, the study conducted in Singapore indicated an energy consumption of 160 kWh/100 km in similar electric buses [22]. Regarding diesel bus consumption in urban driving cycles, despite diesel engine manufacturers claiming efficiencies of up to 40%, actual measured efficiency ranges from 21% to 26% [29]. Correspondingly, fuel consumption falls within the range of 35–50 L/100 km (350–500 kWh/100 km). In the specific case of buses in Gijón, the urban transport company reports an overall consumption of around 50 L/100 km (500 kWh/100 km) [1].

Table 5. Calculated energy consumption and associated CO₂ emissions ¹.

Powertrain	Energy (kWh/100 km)				Emissions (kgCO ₂ /100 km)			
	L02	L10	L15	SORT 1	L02	L10	L15	SORT 1
ICE	484 (430)	458 (415)	498 (445)	515 (460)	150 (133)	142 (129)	154 (138)	160 (143)
EM	165 (160)	161 (155)	161 (155)	191 (187)	45 (43)	43 (42)	43 (42)	52 (50)

¹ Values in brackets correspond to the modified driving cycles with $v_{max} = 30$ km/h.

4. Discussion

The bus commercial speed is defined as the average journey speed of public transport services between two points, including any delay at stops. It is one of the most influencing indicators of public transport quality of service and it is known to be strongly correlated to the frequency and duration of stops [22,23]. This is the case for the real bus lines in this study since the higher the frequency of stops, the lower the commercial speed (L10: $v_{com} = 12.7 < L15: v_{com} = 14.7 < L02: v_{com} = 14.9$ km/h). Additionally, the average velocities during motion and the average decelerations follow the same trend. These results are in alignment with the overall results for the city buses since the overall commercial speed has been in the range of 13.7–14.2 km/h during the last decade [1]. Figure 5a shows the total stops per km vs. commercial speed for the lines in this study compared with the published results [17,18]. The commercial speeds of L02, L10, and L15 are in the lower range, comparable to SORT 1, but slightly higher than expected when considering the stops per km. This is due in part to the comparatively short duration of stops as can be seen in Figure 5b. Consequently, SORT 1 is a good cycle for comparison, although, in small- and mid-sized cities, shorter stops can be expected.

The speed limitation of 30 km/h leads to increased cruising periods but elevates the average accelerations and decelerations. The primary findings for synthetic cycles are detailed in Table 4. Notably, total travel times increase by 3 to 10 min, depending on the original velocity profile and the distance. For the SORT 1 cycle, with an original maximum velocity of 40 km/h, a 25% speed limit reduction causes a 3% reduction in commercial speed. Conversely, a 40% speed limit reduction in real cycles causes a 6 to 10% decrease in commercial speed. Speed limits significantly impact the bus commercial speed, but the precise effect depends on several factors. In many cities, it is accepted that restricting the peak bus speed to less than 40 km/h does not hinder operational performance [30].

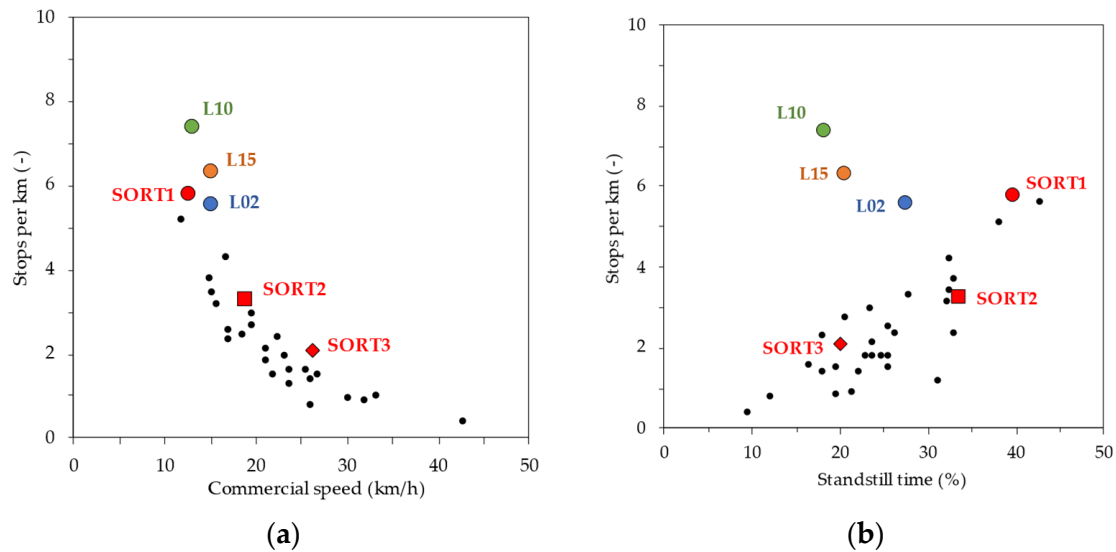


Figure 5. Stop frequency vs. commercial speed (a) and vs. standstill time (b). Small dots represent statistical data of worldwide operators from [18].

As derived from the energy conservation principle for a closed driving cycle, the energy consumed by the vehicle is utilized to overcome dissipative resistances. These resistances comprise rolling, aerodynamic, and energy dissipation during braking. This conceptualization allows for evaluating which characteristics of driving cycles and powertrains have a greater impact on the final energy consumption. Figure 6 illustrates the breakdown of energy dissipation for the four basic driving cycles. For this analysis, the mass of the ICE bus is considered. It is observed that the rolling resistance is nearly constant since it is proportional to the component of the weight that is perpendicular to the road. Given that the considered gradients do not exceed 10%, the normal component is virtually the same for all the cases. Concerning the aerodynamic resistance, its contribution is small, as urban buses, despite having a large frontal area and less favorable aerodynamic coefficients, exhibit low travel speeds, resulting in small aerodynamic resistance values. Nevertheless, differences among cycles exist, and, in general, it is noted that a higher speed leads to increased aerodynamic resistance. However, in a principal component analysis, it can be assumed with minimal error that the sum of the rolling resistance and braking resistance does not vary significantly from one cycle to another. Consequently, differences in energy demand primarily stem from braking usage. In this regard, the driving cycle, which includes velocity and gradient profiles, will have the more significant influence. As depicted in Figure 6, braking energy alone explains the energy consumption differences among the different lines for the ICE powertrain. For the case of EM, since braking is regenerative, and only a part of this energy is dissipated, the differences are much more subdued.

To analyze how the different characteristics of the driving cycles affect the energy dissipated during braking, its distribution along the cycles is examined. Figure 7 illustrates the fraction of the route covered in discrete segments of acceleration and gradient during braking periods ($a_t < 0$). The fraction of the traveled distance during braking under specific acceleration and gradient conditions is indicated. Additionally, a family of a - α curves is shown, representing the specific braking energy for a 13,000 kg mass vehicle assuming a constant rolling–aerodynamic resistance of 37 kWh/100 km. The slope of these curves indicates that the resistance of a 10% gradient route is roughly equivalent to an acceleration of 1 m/s². Furthermore, the total resistance considered for rolling and aerodynamics compensates for gradients of 1% or accelerations of 0.1 m/s², or any other equivalent combination.

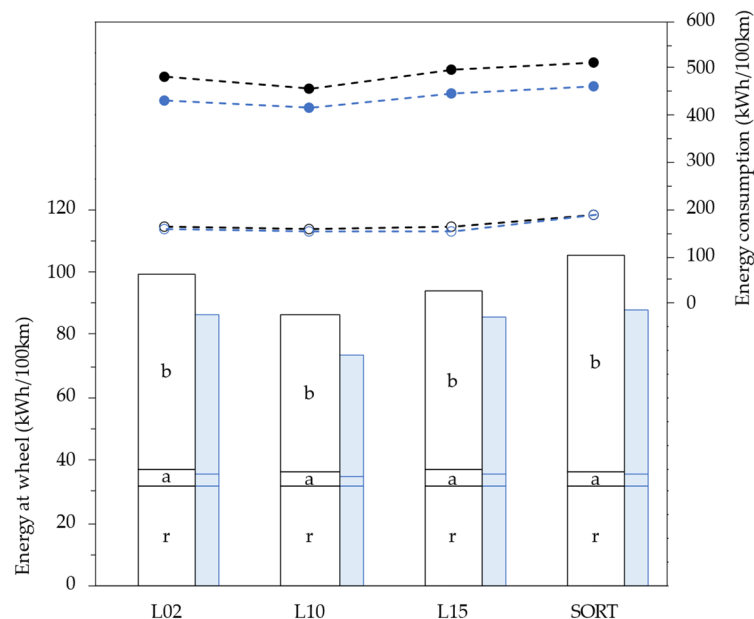


Figure 6. Energy consumption at the motor (solid dots for ICE; open dots for EM) and energy demand at wheel (bars) indicating rolling (r), aerodynamic (a), and braking (b) contributions. The elements represented in blue correspond to the semi-synthetic cycles with $v_{max} = 30$ km/h.

Figure 7 demonstrates how the cycle characteristics determine the required braking energy and, consequently, the energy demand. In comparative terms, the L10 route involves lower accelerations and gradients than lines L02 and L15. Additionally, line L02 frequently experiences higher accelerations but lower gradients than L15. As a result, L10 will have lower braking than lines L02 and L15. This is further highlighted in the summary graph, which shows, for each cycle, the overall specific braking energy. It is observed that, indeed, the braking energy of lines L02 and L15 is higher than that of L10 (≈ 145 vs. 135 kWh/100 km). When comparing lines L02 and L15, a higher or lower acceleration is compensated by a lower or higher gradient, respectively. Consequently, braking energy is similar in both lines. Finally, it is noted that SORT 1 dissipates more energy due to braking (295 kWh/100 km) than the real cycles. Despite not considering road gradients, the deceleration during braking exceeds 0.8 m/s², a value rarely reached in the real cycles. It must be noted that the specific braking energy values shown in Figure 7 correspond to segments where braking is utilized ($e_t < 0$). When these specific energies are weighted by the braking rate (roughly 40%; Table 4), the overall specific braking energies in Figure 6 are obtained.

Figures 6 and 7 also allow us to assess the dissipated energy during braking for the semi-synthetic cycles. Limiting the speed to a maximum of 30 km/h significantly reduces the braking intensity in real cycles. This reduction is much less significant in the case of the SORT 1 cycle, although, as indicated in Table 4, the percentage of the route where brakes are used decreases by 20%. Figure 7 shows that, in all cycles, uphill braking is significantly reduced, and brakes are primarily used to limit accelerations during descents. The energy demand at the wheel for semi-synthetic cycles is shown in blue in Figure 6. The rolling resistance does not change, but the aerodynamic resistance and the braking energy are reduced, on average, by 24% and 20%, respectively. The overall energy demand decreases by 13% on average. The final energy consumption decreases by 10% for the ICE powertrain and only by 3% for the EM powertrain.

The former analysis provides an interesting comparison that can guide decisions for both service providers and users. Firstly, it is observed that the reduction in energy consumption provided by the electric powertrain is greater for L15 (68%) than for L02 (66%) and L10 (65%) and higher than predicted for the SORT 1 cycle (63%). This is a crucial factor in prioritizing this line in a progressive deployment of electric transportation. Other factors,

such as the ease of installing charging points at the route terminus and service headway, must also be considered. In this case, L15 would be also more advantageous because the end terminus is on the outskirts, facilitating the installation of charging points.

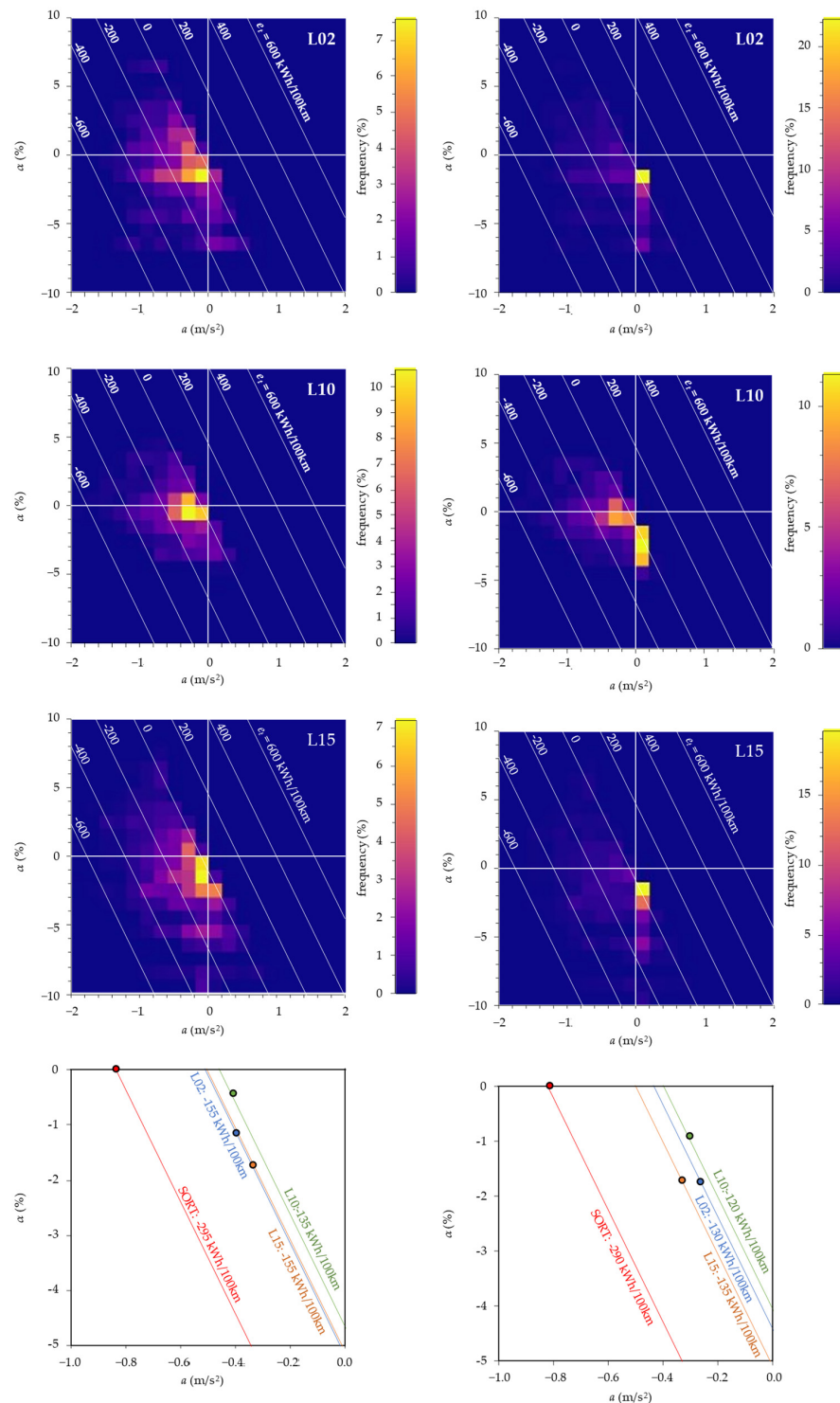


Figure 7. Relation between braking energy and driving cycle characteristics (gradient α vs. acceleration a) for braking periods ($e_t < 0$) in normal cycles (**left**) and semi-synthetic cycles with $v_{max} = 30$ km/h (**right**). Color contours represent the frequency of given conditions during braking periods. The constant e_t curves (white) are computed for a 13 t vehicle with 37 kWh/100 km resistance due to aerodynamic and rolling resistances. Bottom plots represent the average condition for each cycle.

On the other hand, the conducted analysis can provide an evaluation of energy and emissions associated with passenger transport, guiding them in making decisions about the recommended route when several options are possible. Table 6 presents a sample case for a journey between Institutes Square (red dot in Figure 1) and Hospital (east terminus) that can be undertaken using different lines. In this case, although the specific energy consumption is lower for L15, the covered distance for L02 is much shorter, so the associated energy and emissions are lower. Thus, users are informed about which alternative is more environmentally conscious, allowing them to choose a satisfactory compromise between the time, proximity to stops, and environmental footprint. This contributes to the fundamental goal of educating citizens in making more sustainable decisions.

Table 6. User advisory information on a sample journey.

Option	Walking		Bus			
	Time (Min)	Distance (m)	Time (Min)	Distance (km)	Energy ¹ (kWh)	Emissions ¹ (kgCO ₂)
L02 _{ICE}	4	260	15	5.8	0.81	0.25
L10 _{ICE}	2	150	33	7.7	1.06	0.33
L15 _{ICE}	2	150	29	6.5	0.84	0.26

¹ Values per passenger.

The methodology employed in this research offers a high transferability to other locations for several reasons. Firstly, global cartography is readily available in open access, and GPS measurements are easily obtainable in any other case. Furthermore, the application of this methodology can be facilitated in bus networks equipped with telemetry, whether in open access or not.

While specific results may vary depending on the location and particular characteristics of each transport network, the general conclusions of this study are transferrable. For instance, the findings regarding the impact of the slope and driving style on the energy performance of buses are applicable across different urban environments. Similarly, the expected range of variation in the overall performance of conventional and electric powertrains under real-world conditions can serve as a benchmark for future research and sustainable transportation policies in various sites.

The proposed methodology is also generalizable to private transportation networks that adhere to the VANETs scheme and meet the necessary requirements of robustness, privacy, and security [31–33]. Presently, the practical application of these novel vehicle schemes primarily focuses on the agility of movements and emergency safety. However, a layer for energy efficiency and sustainability can be adopted from the methodology developed in this study.

5. Conclusions

A novel methodology has been applied for assessing the energy consumption of urban bus lines. It has been found that commercial speed varies significantly between equivalent bus lines due to the stop frequency and duration differences. Contrary to expectations, bus lines in the study exhibited higher commercial speeds than anticipated, attributed to the brief stop durations.

The driving style has a minimal impact on commercial speed: a 25% reduction in the speed limit results in a 3% decrease in commercial speed. The analysis shows that energy demand is mainly influenced by energy dissipation during braking, linked to decelerations and negative gradients, with significant differences between equivalent lines.

Energy consumption results are consistent with previous studies and company data. Notably, for current ICE powertrains, there is a significant consumption difference (8%) between lines providing similar services. However, EM powertrains exhibit minor differences due to regenerative braking, resulting in a minimal impact from the speed limit

restrictions on consumption (3% for EM; 10% for ICE). The proposed methodology offers insights to medium-sized cities, emphasizing efficient route prioritization and enhanced user decisions.

Future work will involve the comprehensive application of this methodology to the major bus lines of the city over extended periods, aiming to uncover seasonal effects on energy performance.

Additionally, extending the analysis of sustainability should involve other crucial factors such as noise or emission levels, providing a more complete understanding of the environmental impact of urban bus transportation.

Author Contributions: Conceptualization, J.D.; methodology, J.D. and B.P.; software, B.P.; validation, J.D. and B.P.; investigation, B.P. and J.D.; data curation, B.P.; writing—original draft preparation, J.D. and B.P.; writing—review and editing, J.D. and F.J.F.; visualization, J.D.; supervision, J.D. and F.J.F. All authors have read and agreed to the published version of the manuscript.

Funding: This research received no external funding.

Data Availability Statement: The measured raw data used in this article will be made available by the authors on request. For publicly available data used in this study, refer to the References section.

Acknowledgments: The authors would like to express their sincere appreciation to the Gijón City Council and the Public Urban Transport Company for their invaluable contribution in making publicly available data essential for conducting this study.

Conflicts of Interest: The authors declare no conflicts of interest.

Nomenclature

a	(m/s ²)	Acceleration
A_f	(m ²)	Frontal area of the vehicle
c_d	(-)	Aerodynamic drag coefficient
c_r	(-)	Rolling resistance coefficient
e_m	(J/m)	Energy consumption of the motor
e_t	(J/m)	Specific traction energy
F_a	(N)	Aerodynamic drag resistance
F_g	(N)	Gravity force
F_r	(N)	Rolling resistance
F_t	(N)	Traction force of the powertrain
g	(m/s ²)	Gravity acceleration
h	(m)	Road elevation
i_{gb}	(-)	Gearbox ratio
k	(-)	Gear number
m	(kg)	Effective mass of the vehicle
r_w	(m)	Wheel radius
s	(-)	Distance traveled
t	(s)	Time elapsed
T_m	(N·m)	Motor torque
v	(m/s)	Velocity of the vehicle
α	(rad)	Road gradient
η	(-)	Transmission efficiency
ρ_a	(kg/m ³)	Air density
ω	(rad/s)	Angular speed
avg		average
com		commercial

References

1. Ayuntamiento de Gijón Memoria de Sostenibilidad 2022 EMTUSA. Available online: <https://www.gijon.es/es/publicaciones> (accessed on 21 February 2024).

2. Gómez Ortega, A.; Delgado Jalón, M.L.; Rivero Menéndez, J.Á. A Strategic Analysis of Collective Urban Transport in Spain Using the Five Forces Model. *Investig. Eur. De Dir. Y Econ. De La Empresa* **2014**, *20*, 5–15. [\[CrossRef\]](#)
3. Kivekäs, K.; Lajunen, A.; Vepsäläinen, J.; Tammi, K. City Bus Powertrain Comparison: Driving Cycle Variation and Passenger Load Sensitivity Analysis. *Energies* **2018**, *11*, 1755. [\[CrossRef\]](#)
4. Tong, H.Y. Development of a Driving Cycle for a Supercapacitor Electric Bus Route in Hong Kong. *Sustain. Cities Soc.* **2019**, *48*, 101588. [\[CrossRef\]](#)
5. Bishop, J.D.K.; Doucette, R.T.; Robinson, D.; Mills, B.; McCulloch, M.D. Investigating the Technical, Economic and Environmental Performance of Electric Vehicles in the Real-World: A Case Study Using Electric Scooters. *J. Power Sources* **2011**, *196*, 10094–10104. [\[CrossRef\]](#)
6. Tong, H.Y.; Ng, K. Development of Bus Driving Cycles Using a Cost Effective Data Collection Approach. *Sustain. Cities Soc.* **2021**, *69*, 102854. [\[CrossRef\]](#)
7. Astrain, J.J.; Falcone, F.; Lopez-Martin, A.J.; Sanchis, P.; Villadangos, J.; Matias, I.R. Monitoring of Electric Buses Within an Urban Smart City Environment. *IEEE Sens. J.* **2022**, *22*, 11364–11372. [\[CrossRef\]](#)
8. Datos Abiertos. Available online: <https://www.gijon.es/> (accessed on 21 February 2024).
9. Tran, D.-D.; Barrero, R.; Hegazy, O.; Omar, N.; Van Mierlo, J. An Evaluation Study of Hybrid Energy Storage System for Plug-In Hybrid Electric Buses. In Proceedings of the 2017 IEEE Vehicle Power and Propulsion Conference (VPPC), Belfort, France, 11–14 December 2017; pp. 1–7.
10. Naranjo Lourido, W.; Munoz, L.E.; Pereda, J.E. A Methodology to Obtain a Synthetic Driving Cycle through GPS Data for Energy Analysis. In Proceedings of the 2015 IEEE Vehicle Power and Propulsion Conference (VPPC), Montreal, QC, Canada, 19–22 October 2015; pp. 1–5.
11. Hou, D.; Sun, Q.; Bao, C.; Cheng, X.; Guo, H.; Zhao, Y. An All-in-One Design Method for Plug-in Hybrid Electric Buses Considering Uncertain Factor of Driving Cycles. *Appl. Energy* **2019**, *253*, 113499. [\[CrossRef\]](#)
12. Dabčević, Z.; Škugor, B.; Cvok, I.; Deur, J. A Trip-Based Data-Driven Model for Predicting Battery Energy Consumption of Electric City Buses. *Energies* **2024**, *17*, 911. [\[CrossRef\]](#)
13. Tong, H.Y.; Hung, W.T. A Framework for Developing Driving Cycles with On-Road Driving Data. *Transp. Rev.* **2010**, *30*, 589–615. [\[CrossRef\]](#)
14. Prakash, S.; Bodisco, T.A. An Investigation into the Effect of Road Gradient and Driving Style on NOx Emissions from a Diesel Vehicle Driven on Urban Roads. *Transp. Res. Part D Transp. Environ.* **2019**, *72*, 220–231. [\[CrossRef\]](#)
15. Liu, X.; Ma, J.; Zhao, X.; Du, J.; Xiong, Y. Study on Driving Cycle Synthesis Method for City Buses Considering Random Passenger Load. *J. Adv. Transp.* **2020**, *2020*, e3871703. [\[CrossRef\]](#)
16. Bender, F.A.; Sawodny, O. Development of a Refuse Truck Driving Cycle Collective Based on Measurement Data. *Int. J. Environ. Waste Manag.* **2015**, *15*, 99–113. [\[CrossRef\]](#)
17. UITP SORT & E-SORT Brochures. Available online: <https://www.uitp.org/publications/uitp-sort-e-sort-brochures/> (accessed on 28 February 2024).
18. SORT—Standardised On-Road Tests Cycles. Available online: <http://mohamedmezghani.com/images/stories/site/Brochures/5SORT-2004-ENG.pdf> (accessed on 2 March 2024).
19. Badia, H. Comparison of Bus Network Structures in Face of Urban Dispersion for a Ring-Radial City. *Netw. Spat. Econ.* **2020**, *20*, 233–271. [\[CrossRef\]](#)
20. Durán-Micco, J.; Van Kooten Niekerk, M.; Vansteenwegen, P. Designing Bus Line Plans for Realistic Cases—The Utrecht Case Study. *Expert Syst. Appl.* **2022**, *187*, 115918. [\[CrossRef\]](#)
21. Yazici, A.; Levinson, H.; Ilicali, M.; Camkesen, N.; Kanga, C. A Bus Rapid Transit Line Case Study: Istanbul’s Metrobüs System. *JPT* **2013**, *16*, 153–177. [\[CrossRef\]](#)
22. Gallet, M.; Massier, T.; Hamacher, T. Estimation of the Energy Demand of Electric Buses Based on Real-World Data for Large-Scale Public Transport Networks. *Appl. Energy* **2018**, *230*, 344–356. [\[CrossRef\]](#)
23. Casavola, A.; Gagliardi, G.; Nesci, W. A Quasi-Static Simulation Tool for the Design and Optimization of Hybrid Powertrains. Available online: https://www.researchgate.net/publication/258286462_A_quasi-static_simulation_tool_for_the_design_and_optimization_of_hybrid_powertrains (accessed on 28 February 2024).
24. Mercedes-Benz Autobuses y Autocares: Home. Available online: https://www.mercedes-benz-bus.com/es_ES/home.html (accessed on 28 February 2024).
25. Commercial Vehicle Solutions—ZF. Available online: <https://www.zf.com/products/en/cv/home/cv.html> (accessed on 28 February 2024).
26. Ministerio de la Presidencia, Relaciones con las Cortes y Memoria Democrática. In *Real Decreto 970/2020, de 10 de Noviembre, Por El Que Se Modifican El Reglamento General de Circulación, Aprobado Por Real Decreto 1428/2003, de 21 de Noviembre y El Reglamento General de Vehículos, Aprobado Por Real Decreto 2822/1998, de 23 de Diciembre, En Materia de Medidas Urbanas de Tráfico*; Gobierno de España: Madrid, Spain, 2020; Volume BOE-A-2020-13969, pp. 98638–98643.
27. IDEA. *Factores de Emisión de CO₂ y Coeficientes de Paso a Energía Primaria de Diferentes Fuentes de Energía Final*; IDEA: Madrid, Spain, 2014.
28. MITECO. *Factores de Emisión, Registro de Huella de Carbono*; MITECO: Madrid, Spain, 2023.

29. Nylund, N.-O.; Erkkilä, K.; Hartikka, T. Fuel Consumption and Exhaust Emissions of Urban Buses. Available online: <https://publications.vtt.fi/pdf/tiedotteet/2007/T2373.pdf> (accessed on 28 February 2024).
30. Gandhi, S.; Tiwari, G.; Fazio, J. Comparative Evaluation of Alternate Bus Rapid Transit System (BRTS) Planning, Operation and Design Options. *J. East. Asia Soc. Transp. Stud.* **2013**, *10*, 1292–1310.
31. Liu, Z.; Wan, L.; Guo, J.; Huang, F.; Feng, X.; Wang, L.; Ma, J. PPRU: A Privacy-Preserving Reputation Updating Scheme for Cloud-Assisted Vehicular Networks. *IEEE Trans. Veh. Technol.* **2023**, 1–16. [[CrossRef](#)]
32. Liu, Z.; Weng, J.; Ma, J.; Guo, J.; Feng, B.; Jiang, Z.; Wei, K. TCEMD: A Trust Cascading-Based Emergency Message Dissemination Model in VANETs. *IEEE Internet Things J.* **2020**, *7*, 4028–4048. [[CrossRef](#)]
33. Liu, Z.; Weng, J.; Guo, J.; Ma, J.; Huang, F.; Sun, H.; Cheng, Y. PPTM: A Privacy-Preserving Trust Management Scheme for Emergency Message Dissemination in Space–Air–Ground-Integrated Vehicular Networks. *IEEE Internet Things J.* **2022**, *9*, 5943–5956. [[CrossRef](#)]

Disclaimer/Publisher’s Note: The statements, opinions and data contained in all publications are solely those of the individual author(s) and contributor(s) and not of MDPI and/or the editor(s). MDPI and/or the editor(s) disclaim responsibility for any injury to people or property resulting from any ideas, methods, instructions or products referred to in the content.